Published in final edited form as:
Langmuir. 2010 July 20; 26(14): 12140–12146. doi:10.1021/la101674b.

Spatial variation of charge and sulfur oxidation state in a surface gradient affects plasma proteins adsorption

Yong-Xue Ding, **Seth Streitmatter**, **Bryon E. Wright**, and **Vladimir Hlady***
Department of Bioengineering, University of Utah, Salt Lake City, UT 84112

Abstract

A gradient of negative surface charge based on 1-D spatial variation from surface sulfhydryl to mixed sulfhydryl-sulfonate moities was prepared by controlled UV oxidation of 3-mercaptopropylsilane monolayer on fused silica. Adsorption of three human plasma proteins, albumin (HSA), immunoglobulin G (IgG), and fibrinogen (Fgn) onto such surface gradient was studied using spatially-resolved total internal reflection fluorescence (TIRF) and autoradiography. Adsorption was measured from dilute solutions equivalent to 1/100 (TIRF, autoradiography), and 1/500 and 1/1000 (autoradiography) of protein's physiological concentrations in plasma. All three proteins adsorbed more to the non-oxidized sulfhydryl region than to the oxidized, mixed sulfhydryl-sulfonate region of the gradient. In the case of HSA the adsorption contrast along the gradient was largest when the adsorption took place from more dilute protein solutions. Increasing the concentration to 1/100 of protein plasma concentration eliminated the effect of the gradient on HSA adsorption and to the lesser extent on IgG adsorption. In the case of Fgn the greatest adsorption contrast was observed at the highest concentration used. Based on adsorption kinetics, the estimated binding affinity of HSA for the sulfhydryl region what twice the affinity for the mixed sulfhydryl-sulfonate region of the gradient. For IgG and Fgn the initial adsorption was transport-limited and the initial adsorption rates approached the computed flux of the protein to the surface.

Keywords

Protein adsorption; Surface gradient; Albumin; Immunoglobulin G; Fibrinogen; TIRF; Autoradiography

INTRODUCTION

The response of blood to man-made material surfaces is one of the most difficult problems in the biocompatibility. Adsorption of blood proteins to biomaterials in vivo is a trigger of the coagulation cascade, platelet adhesion, and thrombus formation [1,2]. While new biomaterials with improved compatibility are being continuously developed, no truly hemocompatible biomaterials have emerged [3,4]. Some general rules about hemocompatibility have been established: - it is generally accepted that surface characteristics such as wettability, charge, roughness, topography, and chemistry play an important role in determining the fate of implanted biomaterials [5,6,7]. However, the molecular-level information about the inter-relation between a surface property and protein adsorption remains largely unavailable. To obtain such information one needs to understand biomaterial's surface chemistry and microstructure on a sub-μm, protein-size, scale. Here

*Corresponding author: Vladimir Hlady, Professor, Department of Bioengineering, 20 S. 2030 E., Rm. 108A, University of Utah, Salt Lake City, UT 84112, vladimir.hlady@utah.edu, Tel: 801-581-5042, Fax: 801-585-5151.

lies the problem: the task of studying the effect of each surface property on protein adsorption, using a range of biomaterials, could be tedious and time consuming, if not impossible. To circumvent this problem several groups have developed model surfaces where chemical composition or physical characteristics, such as density of grafted polymers or length of the polymer chains, vary in 1D or 2D. These so-called “gradient surfaces” have been the subject of two recent reviews [8,9]. In addition to mimicking the naturally present gradients, the gradient surfaces have been an effective research tools for screening of the influence of a given surface parameter on interfacial events. The use of gradient surfaces has been very popular in studying protein-surface interactions [10–19], immobilizing macromolecules, proteins and peptides [20–22], and investigating bacteria, cell or platelet adhesion [23–26].

In the case of chemical gradients, the substrate surface carries a gradually changing surface chemistry, which is responsible for spatial variations of surface properties such as surface energy, polarity, or charge. This spatial variation creates a contrast, which could be large, like between wetting and non-wetting regions of a surface gradient. Because protein adsorption is strongly affected by the surface hydrophobicity, we and others have extensively used the gradients of wettability to study protein adsorption [10–14,16–19].

Protein adsorption is also very sensitive to surface charge [6,15,27]. The challenge is how to study the effects of surface charge on protein adsorption separately from the effects of other surface parameters present in the gradient. To this end we have recently designed a method to prepare a surface charge gradient starting from an initially uniform monolayer on fused silica of 3-mercaptopropyl-trimethoxysilane (MTS) which is selective oxidized using a controlled UV exposure [28]. The result of the UV exposure is a gradient of surface sulfhydryl groups and a counter-gradient of sulfonate groups: a linear gradation of the average oxidation state in the sulfur-containing terminal group of the MTS moiety. This subtle change in the oxidation state of sulfur brings to a change of negative surface charge density and the related surface energy. In this study we investigated how the gradient of negative surface charge influences adsorption of three blood proteins: albumin (HSA), immunoglobulin G (IgG) and fibrinogen (Fgn). These three proteins play an important role in biomaterials hemocompatibility [1–5]: - adsorbed HSA is considered to have protective action [29], - IgG participates in host’s immune response [30], and - adsorbed Fgn is know to induce platelet activation [31]. In order to capture the effects of negative surface charge gradient on protein binding the concentration of proteins was kept low, ranging from 1/1000 – 1/100 of their physiological concentration in plasma.

MATERIALS AND METHODS

The preparation of the gradient followed the previously established procedure [28]. Briefly, fused silica (FS, Ted Pella) were cleaned and activated using a three-step process: 10 minute oxygen plasma treatment, (Plasmod, Tegal Inc., 50 W @ 200 mTorr), 2 hour “piranha” bath, and a second 10 minute oxygen plasma treatment. The clean slides were immediately immersed in fresh 1% solution of 3-mercaptopropyltrimethoxysilane (MTS, United Chemical Technologies, Inc) in dry toluene and reacted for four hours in the dark. After the reaction, the solution was drained and the MTS monolayer slides were sequentially rinsed with toluene, acetone, ethanol, deionized water, and finally dried with filtered nitrogen.

Sulfhydryl-to-sulfonate surface gradients were created by selectively oxidizing the MTS monolayer using controlled UV exposure in a custom-designed motorized oxidation chamber using the edge mask displacement to control the gradient length [28]. In this study, a 1 cm long oxidation gradient was created in the center of the slide, flanked by the oxidized (2 minutes of UV exposure) and non-oxidized (no UV exposure) areas on each side. Thus

created gradients were immediately characterized and/or used in protein adsorption experiments.

Water contact angles were measured on the gradient surfaces at room temperature using a video goniometer (Cam100, KSV). Receding contact angles of about twenty droplets of double-distilled water were measured along the length of the sample. Contact angle hysteresis was estimated by moving a hanging water droplet along the gradient.

A scanning force microscope operating in a force-volume mode (SFM, Explorer, Topometrix) was used to map the adhesion force (i.e. "pull-off" force) on unmodified and oxidized MTS (2 minutes UV irradiation) monolayers. All adhesion measurements were performed in double-distilled water. For the adhesion mapping MTS monolayers were prepared on silicon wafer rather than on fused silica. A silicon nitride tip (nominal radius of curvature, r_{tip} = 20 nm) integral to a rectangular SFM cantilever (MicroMash) was employed as an adhesion probe. The adhesion mapping comprised 2500 (i.e. 50 × 50 sites) consecutive force-displacement cycles made on a 10 by 10 μm^2 area. In this way, the pull-off force was probed at sites 200 nm apart. The maximal load in each cycle was ~15 nN. ImageJ software (W. Rasband, NIH) was used to extract the magnitude of the adhesion force at pull-off. The adhesion forces were calibrated using the nominal cantilever spring constant, k_{sp} = 0.06 Nm^{-1}. The force resolution (100 pN) in the pull-off force measurements was determined by the total displacement made in each cycle and the number of layered images taken by the microscope. The XPS spectra of unmodified, and UV oxidized MTS monolayers on fused silica were recorded using an XPS spectrometer (Axis-Ultra DLD, Kratos) at the University of Utah Nanofab Lab.

Proteins were either labeled with Alexa Fluor® 488 dye (Alexa Fluor® carboxylic acid, succinimidyl ester mixed isomers, Molecular Probes) for TIRF experiments, or with ^{125}I ($Na^{125}I$, GE Healthcare) for autoradiography. Alexa Fluor® 488 dye with was covalently bound to HSA (Sigma), IgG or Fgn (Cabiochem) following the protocol from Molecular Probes [32]. The protein concentrations were measured with the Biorad® protein assay method [33]. The molar degree of protein labeling, calculated from UV-VIS absorbance measured at 280 nm and 460 nm, was determined to be 0.8, 1.4, and 0.7, for HSA, IgG, and Fgn, respectively. For autoradiography experiments HSA, IgG and Fgn were each iodinated with ^{125}I ($Na^{125}I$, GE Healthcare) using chloramine-T (Sigma) as the oxidizing agent [34]. The iodinated protein solution was applied to a PD-10 column to remove the unreacted $Na^{125}I$. The ^{125}I-labeled proteins were used within a week.

The protein adsorption kinetics were measured in a custom-designed TIRF flow cell [12]. The flow cell contained two identical rectangular shape flow channels allowing for two adsorption experiments on the same gradient surface. Fluorescently labeled protein solutions, HSA, IgG, or Fgn, were prepared at 1/100 of their respective plasma concentration in PBS (i.e. 0.4 mg ml^{-1} HSA, or 0.12 mg ml^{-1} IgG, or 0.03 mg ml^{-1} Fgn in PBS, pH 7.4). In each TIRF experiment, the flow channels were pre-filled with PBS that was then replaced with an 11 minute perfusion of protein solution (flow rate = 0.70 ml min^{-1}). This was followed by second perfusion with PBS (time = 11 min) to initiate protein desorption. Unless indicated otherwise, the flow direction was from lower adsorption region to higher adsorption region across the gradient. The fluorescence emission from the surface-bound protein was excited by an evanescent wave created by the total internal reflection of a spatially filtered, expanded Ar^+-ion laser beam (488 nm, 0.5 mW total power). The adsorbed protein fluorescence was imaged using a 50 mm lens (*f*/4, Pentax) onto the slit of a monochromator (1681C, SPEX Industries Inc., *f*/4, 2 mm slit, 300 grooves per mm of grating) and recorded every second by a cooled charged couple device camera (C200,

Photometrics). The fluorescence emitted along the gradient was background-subtracted and corrected for the laser beam power profile.

Each ^{125}I-labeled protein was adsorbed onto the gradient surface using the perfusion protocol identical to the TIRF experiments. In addition to 1/100 of respective plasma concentration each protein was also adsorbed from PBS solutions equivalent to 1/500 or 1/1000 of its plasma concentration. After the completed adsorption-desorption cycle, the adsorbed proteins were fixed with 3 ml of 0.6% glutaraldehyde in PBS solution for 5 minutes. For each protein, a calibration plate with known ^{125}I-protein surface concentration was prepared on a uniform MTS slide. The gradient surface with adsorbed ^{125}I-protein and the calibration slide were placed in a plastic bag and brought into contact with a Kodak MS film in a light-tight cassette, and exposed for 30 hrs at −70°C [35]. The exposed film was processed in an automated developer system and digitized using a high-resolution 16-bit scanner.

The quantification of autoradiography protein adsorption followed the procedure outlined previously [36]. The background subtracted film density (gray value) of each protein concentration from the calibration plate image was used to establish the calibration plot (gray value vs. protein mass). The adsorbed amount of protein was calculated from the gradient film density profile using the calibration plot. Autoradiography measured adsorption profiles were used to quantify the fluorescence data. A conversion factor, which related the protein surface concentration profile (as determined by autoradiography) to the fluorescence intensity profile measured at the end of the adsorption-desorption cycle in TIRF experiment was back-propagated in time to convert the fluorescence intensity kinetics into protein surface mass concentration vs. time.

RESULTS

Surface characterization

Water contact angles were used to visualize the length of the surface charge gradient. The receding water contact angles measured on the unmodified MTS monolayer were 60 ± 3°. After 2 minutes exposure to the UV irradiation power of ~10 mW cm^{-2}, the contact angle decreased to ~30 ± 4°. Fig. 1 shows the receding water contact angle as a function of gradient position for 2 minutes of UV irradiation. The contact angle hysteresis in the middle of the gradient was between 18 – 25°. The 4 minutes UV irradiation and controls data are included in Fig 1 for comparison.

The spatial distribution of “pull-off” adhesion forces on the UV oxidized MTS and control surfaces is illustrated by the AFM adhesion maps (10 by 10 μm^2) and respective histograms of adhesion forces (Fig. 2A). The control MTS monolayer showed the average adhesion force of 0.5 nN. The oxidized MTS (2 minutes UV irradiation) showed a much broader range of adhesion forces centered at 3.4 nN. The XPS S2p spectra of the MTS monolayers are shown in Fig. 2B. Reaction of fused silica with 1% MTS solution resulted in the appearance of a strong S2p peak at 163.5 eV confirming the presence of –SH containing monolayer. The elemental XPS analysis showed ~2 atomic % of S, which is expected for MTS monolayer [37]. After 2 minutes of UV irradiation, the 163.5 eV peak decreased in magnitude while a new peak emerged at the binding energy of 167.5 eV. The higher binding energy peak indicated that a fraction of sulfur atoms from the –SH groups have reacted with oxygen and formed sulfonate moieties [38]. The fraction of sulfur in the oxidized state, defined as the ratio of higher energy peak area to total S2p area, was ~0.3 indicting that only a partial oxidation of surface thiols occurred on the UV irradiated side of the gradient. In the previous study we used 4 minutes of UV oxidation, which resulted in smaller water contact

angles (Fig 1) and a larger fraction of oxidized S, but also in a decrease of atomic % of C and S, presumably due to the scission of the MTS bonds [28,37].

HSA adsorption

Typical results of HSA adsorption onto the sulfhydryl-to-sulfonate surface gradient are shown in Fig. 3. Fig. 3A shows the adsorption-desorption kinetics of Alexa 488-HSA measured in TIRF experiments. Each kinetic trace was an average over a 50 μm wide region on non-oxidized MTS, oxidized MTS regions, and in the middle of the gradient. The reproducibility of the fluorescence intensity in repeated TIRF experiments was +/−7% (estimated at each side of the gradient). Fig. 3B shows the autoradiography image of the calibration plate and the calibration plot for ^{125}I-HSA. The adsorption profiles of ^{125}I-HSA along the gradient are shown in Fig. 4C (lower panel) with the position measured from the middle of the gradient. Autoradiography images of ^{125}I-HSA adsorbed along the entire flow channel are shown in Fig. 3C (upper panel). At the highest ^{125}I-HSA solution concentration, (0.4 mg ml^{-1}) the presence of the surface gradient had very little influence on the adsorbed amount, Γ: it changed only from 0.83 to 0.78 μg cm^{-2} (~2.4% change) across the gradient. The effect of the gradient was more pronounced for the two lower concentrations. Adsorption from 0.04 mg ml^{-1} solution (1/1000) resulted in a change from Γ_{HSA} = 0.62 to Γ_{HSA} = 0.17 μg cm^{-2} (~72% change) from the non-oxidized to oxidized end, and a similar trend was found for the adsorption from 0.2 mg ml^{-1} solution (1/500) where the Γ_{HSA} changed from 0.67 to 0.39 μg cm^{-2} (~42% change) along the gradient.

The autoradiography calibrated TIRF adsorption-desorption kinetics of HSA are shown in Fig. 3D. Adsorption on the oxidized MTS region did not reach a steady-state at the end of the 11 minute adsorption cycle. In contrast, the adsorption on the sulhydryl MTS region leveled at 0.9 μg cm^{-2}. The initial Alexa 488-HSA adsorption rate on the downstream sulhydryl region, $d\Gamma_{HSA}/dt$, was 7.9•10^{-3} μg cm^{-2} s^{-1}, which was faster than on the upstream oxidized MTS region ($d\Gamma_{HSA}/dt$ = 2.8•10^{-2} μg cm^{-2} s^{-1}). At the center of the gradient an adsorption rate of 1.3•10^{-3} μg cm^{-2} s^{-1} was observed. During the desorption part of the experiment ~10% of adsorbed protein were washed away from each of the three gradient positions.

IgG adsorption

Autoradiography calibrated TIRF adsorption of IgG onto the surface charge gradient is shown in Fig. 4A. Unlike HSA, the presence of the surface charge gradient had no effect on the initial IgG adsorption rate. On the both ends of the gradient, the initial adsorption rates were similar ($d\Gamma_{IgG}/dt$ ~ 7.1•10^{-3} – 8.4•10^{-3} μg cm^{-2} s^{-1}) indicating that the initial IgG binding might be transport-limited. Although final adsorption was higher on sulfhydryl vs. sulfonate-containing MTS region, a true steady state adsorption was not reached for any of the three positions. Desorption by buffer solution resulted in a removal of a small fraction of adsorbed IgG (< 10%).

Fig. 4B shows the typical ^{125}I-IgG adsorption profiles. The adsorbed ^{125}I-IgG from solution of 0.012 mg ml^{-1} (1/1000 of plasma concentration) showed the adsorption contrast ranging from Γ_{IgG} = 0.39 μg cm^{-2} at the non-oxidized MTS to Γ_{IgG} = 0.16 μg cm^{-2} at the oxidized MTS side of the gradient (a 59% change). When ^{125}I-IgG concentration was increased to 1/500 of its respective blood plasma level, the ^{125}I-IgG surface showed a 42% change across the gradient. For ^{125}I-IgG concentration of 0.12 mg ml^{-1}, Γ_{IgG} changed only by 30%, decreasing from Γ_{IgG} = 0.46 to Γ_{IgG} = 0.32 μg cm^{-2} along the gradient. Compared with ^{125}I-HSA, adsorbed ^{125}I-IgG showed a similar pattern with more protein adsorbed to the non-oxidized than to the oxidized MTS gradient regions.

Fgn adsorption

The adsorption of Fgn to the sulfhydryl-to-sulfonate surface gradient is shown in Fig. 5. Fig. 5A shows the autoradiography calibrated adsorption-desorption kinetics of Alexa 488-Fgn measured in TIRF experiments.* The calibration of the TIRF kinetics resulted in different steady state adsorption levels while the same initial adsorption rates indicated that the initial Fgn adsorption might be transport-limited. Desorption of Fgn by PBS solution was negligible. Fig. 5B (upper panel) shows typical ^{125}I-Fgn autoradiography images of the entire flow channel. The adsorption profiles of ^{125}I-Fgn along the gradient are shown in Fig. 6B, lower panel. The contrast between ^{125}I-Fgn adsorption on non-oxidized vs. oxidized MTS regions was largest from solution concentrations of 0.03 mg ml^{-1} (equivalent to 1/100 plasma concentration) and slightly less from 0.015 mg ml^{-1} (1/500). The adsorption from 0.003 mg ml^{-1} solution (1/1000) was around 0.1 μg cm^{-2} and no variations of the adsorbed amount along the gradient were detected.

DISCUSSION

Over the past years, several techniques have been used to create gradient surfaces for bio-interactions studies. The techniques for preparing these chemistry gradient surfaces included counter-diffusion, density gradient method, radio frequency plasma discharge, corona discharge, and others [8,9]. We have developed a versatile approach in creating surface charge gradients based on an initially uniform MTS monolayer that is partially oxidized by UV [28]. The extent of the surface oxidation and the fraction of oxidized sulfhydryl groups were directly related to UV irradiation time [37]. In this study we used 2 minutes of UV irradiation which, based on the XPS results, oxidized ~1/3 of the monolayer sulfhydryl groups (Fig 2B). For a close-packed monolayer of MTS, with the area of 0.50 nm^2 per weakly ionized –SH group with solution pKa 8.5 [39], the surface charge density at pH 7.4 was estimated to be ~0.007 C/m^2 for the non-oxidized MTS and ~0.030 C/m^2 for oxidized MTS regions, respectively. Thus, the oxidation of the surface sulfhydryl groups has generated a gradient of surface charge, from weakly charged sulfhydryl groups to a mixture of strongly charged sulfonate (1/3 fraction) and sulfhydryl groups (2/3 fraction); a gradient which also displayed the gradient of surface wettability (Fig. 1) and surface energy (Fig. 2A). These gradient characteristics resulted from a change in the oxidation state of sulfur while the other chemistry of the monolayer remained largely unchanged.

An easy way to verify the existence of such gradient was by measuring water contact angles (Fig. 1). The water contact angle hysteresis (18 – 25° in the middle of the gradient) indicated that the local surface chemistry was heterogeneous [40]. The uniformity of the MTS monolayers was also visualized using adhesion force maps (Fig. 2A). The adhesion “pull-off” force is related to the interfacial energy of MTS monolayers and thus to the water contact angle. The adhesion force map for the unmodified MTS monolayer showed only a few random spots with higher adhesion (Fig. 2A, MTS image) with the adhesion force histogram width (FWHM) of ~ 1.2 nN. After 2 minutes of UV irradiation, adhesion forces increased significantly and so did the heterogeneity: - the force histogram width (FWHM) increased to ~3.4 nN. The irradiation effects were spatially random as evidenced by the absence of any regular patterns in the adhesion force map of the oxidized MTS monolayer (Fig 2A, ox-MTS image). That the UV irradiation made the MTS surface more heterogeneous which was also supported by the XPS data (Fig 2B).

The adsorption of three plasma proteins showed that the variation in the surface charge and the oxidation state of sulfur had significant effect on protein binding, especially from dilute

*Alexa 488-Fgn solution was perfused from the non-oxidized to oxidized MTS side of the gradient.

solutions. The interactions between a protein and a solid surface is affected by a range of different interactions, from the ubiquitous van der Walls and electrostatic interactions to entropy-driven dehydration of both protein and solid surface and eventual rearrangements of protein structure [5,6]. In addition to these physical interactions, there was also a possibility of chemical interactions: surface sulfhydryl groups were capable of forming disulfide bonds with cystein's side chain in proteins. Both sulfhydryl and sulfonate groups have biological relevance: sulfonate groups are present in many natural macromolecules such as heparin and various glycosaminoglycans that also interact with proteins and sulfhydryl groups as mentioned above. In the present study, no reducing agents such as dithiothreitol were used in the adsorption experiments so that the adsorption followed by the creation of covalent bond between protein and sulfhydryl group could not be ruled out.**

All three proteins have their isolelectric points below pH 7 [1]; i.e. their overall charge was negative at the experimental conditions used in this study. The adsorption behavior of all three proteins followed the same pattern: more adsorption on the weakly charged sulfhydryl groups side of the gradient than on the strongly charged mixture of sulfhydryl and sulfonate groups. However, each proteins also contained positively charged amino acid side chains exposed on their outside surfaces, which could favor the adsorption interaction with negatively charged gradient [41,42]. The adsorption contrast was probably affected by the presence of 0.15 M NaCl which screens the electrostatic interactions, however, the role of ionic strength was not further investigated.

Adsorption kinetics can provide an estimate of protein-surface binding affinity. Table 1 summarizes the adsorption parameters for the three proteins measured at the concentrations equivalent to 1/100 of their respective plasma concentrations. For IgG and Fgn the initial adsorption rates did not vary much with the upstream vs. downstream flow positions. This is expected for a transport-limited adsorption where the flux of the protein to the surface, J_p, can be calculated by the Leveque equation [43]:

$$J_p=[\Gamma(\frac{4}{3})]^{-1}9^{-\frac{1}{3}}(\frac{6q}{b^2wlD_p})^{\frac{1}{3}}D_pc_p \quad (1)$$

where D_p is the diffusion coefficient of the protein, c_p is protein bulk concentration, Γ(4/3) is the gamma function of 4/3, l is the distance along the rectangular flow channel measured from its entrance, b is the thickness of the flow channel, q is the volumetric flow rate of protein solution and w is the width of the flow channel. It is instructive to compare the maximum possible adsorption rate, so-called "Leveque rate" [43–45], with the highest initial adsorption rate for the three positions along the surface gradient.*** For both IgG and Fgn, the initial adsorption rates agreed well with the calculated "Leveque rates." For IgG the initial rate was ~4/5 of the "Leveque rate" in the upstream sulfonate region of the gradient, ~9/10 in the center of the gradient and ~19/20 in the downstream sulfhydryl region. Thus, the IgG adsorption seems to be transport-limited everywhere except at the most upstream, sulfonate-rich position of the gradient. In the case of Fgn, the initial adsorption rate was ~9/10 of the "Leveque rate" at both the upstream sulfhydryl region and the center of the

**One advantage of sulfhydryl-to-sulfonate gradient is that the remaining sulfhydryl groups can be reacted with another compound thus further changing the chemical nature of the surface gradient [V. Hlady, unpublished data].

***One additional benefit of such binding rate comparison is the check on the applicability of the conversion factor used in the calibration of TIRF fluorescence. Since all parameters in the rhs of Eq. 1 are known, the agreement between the autoradiography-calibrated initial adsorption rate and the "Leveque rate" also indicates that the quantum yield of Alexa488 dye was constant throughout the adsorption/desorption process.

gradient and ~1 in the downstream sulfonate region. As expected for such large protein, the process of adsorption was initially transport-limited.

Only in the case of HSA the initial adsorption rate was a smaller fraction of the "Leveque rate": ~1/5 in the upstream sulfonate region of the gradient, ~1/3 in the center of the gradient and ~¾ in the downstream sulfhydryl region, thus supporting the conclusion that the HSA adsorption was initially not transport-limited. We estimated that this protein has a higher affinity for the sulfhydryl region than for the mixed sulfonate-sulhydryl region of the gradient as shown by the ratios of its initial rate and the desorption rate: $k_{on\_initial}/k_{off}$ ~1 μg cm^{-2} for sulfhydryl vs. ~0.5 μg cm^{-2} for the oxidized MTS region, respectively. Because these binding affinity differences are primarily determined by the initial rates, they probably reflect the protein-surface interactions at low surface coverage, i.e. in the absence of lateral protein-protein interactions. In other words, the binding affinity is very likely to be a function of surface coverage. This may explain the finding that the maximum adsorption of HSA on all three regions of the gradient was quite similar, $\Gamma_{HSA} = 0.76 - 0.83$ μg cm^{-2}. For IgG or Fgn, similar evaluation of the binding affinity from the initial adsorption and desorption rates could not be made due to the transport-limitation of the initial rates. In these two cases, the adsorption kinetics transited from an initial transport-limited regime to an adsorption-limited regime at higher surface coverage.

In the present study we have used labeled proteins. Although the degree of labeling of proteins with Alexa488 dye was intentionally kept very low to prevent the self-quenching of the dye, the addition of the dye might have changed the "conformationally sensitive" protein such as Fgn [46] and thus influenced its adsorption behavior. Similarly, iodination of protein's tyrosine residues with ^{125}I could also have produced the change in their adsorption pattern. However, the similarity between the TIRF and autoradiography profiles indicated that the adsorption behavior of dye- and ^{125}I-labeled proteins was not that much different.

The gradation of the sulfur oxidation state and negative surface charge along the gradient influenced protein adsorbed amount more at lower solution concentrations than at higher concentrations, except for Fgn. For IgG and HSA the effect of the electrostatics increased the adsorption contrast at lower protein concentrations. Increasing the protein solution concentration up to 1/100 of their concentration in plasma diminished the effect of the gradient, especially for HSA. In the case of IgG it is possible that the same would happen as its concentration approached its concentration in plasma. The effect of the gradient was not diminished at higher Fgn concentration: - the protein adsorbed to all surfaces with the maximum transport-limited rate regardless of the surface chemistry and yet the adsorbed amounts were different along the gradient. The present results agree with the reports that the adsorbed Fgn amount increases with increasing contact angle [10] and decreasing negative surface potential [47]. What would happen if the concentration of Fgn is further increased to its physiological level is difficult to predict. However, one may speculate that the lower adsorption of Fgn onto sulfonate-containing interfaces could be the reason for improved hemocompatibility of biomaterials such as sulfonated polyurethanes [48].

CONCLUSIONS

Adsorption of three human plasma proteins: albumin, immunoglobulin G, and fibrinogen onto a negative charge gradient surface was determined by an interplay between the electrostatic interactions and the protein solution concentration. All three proteins adsorbed less to the more negatively charged, mixed sulfonate-sulhydryl region of the gradient than to the non-oxidized, weakly charged sulfhydryl region of the gradient. The adsorption kinetics were used to estimate binding affinity of the proteins for the gradient regions. Because the initial adsorption processes for IgG and Fgn were transport-limited, the estimate was could

be made only for HSA, where the affinity for weakly charged sulfhydryl region was twice as large than the affinity for the more negatively charged, mixed sulfonate-sulhydryl region of the gradient. In the case of HSA and to some degree for IgG, the adsorption contrast along the gradient was largest when the adsorption took place from more dilute protein solutions, presumably due to the dominance of protein-surface interactions over the lateral protein-protein interactions. In the case of Fgn, higher adsorption contrast was observed at the highest Fgn concentration. The low adsorption to sulfonate-containing part of the gradient could be the reason for improved hemocompatibility of sulfonated biomaterials.

Acknowledgments

This study was supported by an NIH grant (R01 HL084586). Authors thank K. Neaman and D. Mishra for the preliminary results on MTS gradients and gratefully acknowledge the discussions with P.F. Kiser on various aspects of gradient surface chemistry.

REFERENCES

1. Andrade JD, Hlady V. Ann. NY Acad. Sci. 1987; 516:158–172. [PubMed: 3439723]
2. Horbett, TA. Biomaterials Science. 2nd ed.. Ratner, BD.; Hoffman, AS.; Schoen, FJ.; Lemons, JE., editors. San Diego: Elsevier Academic Press; 2004. p. 237-246.
3. Sefton, MV.; Gemmell, CH. Biomaterials Science. 2nd ed.. Ratner, BD.; Hoffman, AS.; Schoen, FJ.; Lemons, JE., editors. San Diego: Elsevier Academic Press; 2004. p. 456-470.
4. Ratner BD, Bryant SJ. Annu. Rev. Biomed. Eng. 2004; 6:41–75. [PubMed: 15255762]
5. Andrade, JD., editor. Surface and Interfacial Aspects of Biomedical Polymers Vol. 2 Protein Adsorption. New York: Plenum Press; 1985. p. 1-347.
6. Norde W. Adv. Colloid Interface Sci. 1986; 25:267–340. [PubMed: 3333131]
7. Kim MS, Khang G, Lee HB. Prog. Polym. Sci. 2008; 33:138–164.
8. Genzer J, Bhat RR. Langmuir. 2008; 24:2294–2317. [PubMed: 18220435]
9. Morgenthaler S, Zink C, Spencer ND. Soft Matter. 2008; 4:419–434.
10. Elwing H, Welin S, Askendal A, Nilsson U, Lundström I. J. Colloid Interface Sci. 1987; 119:203–210.
11. Elwing H, Gölander C-G. Adv. Colloid Interface Sci. 1990; 32:317–339.
12. Hlady V. Appl. Spectrosc. 1991; 45:246–252.
13. Gölander C-G, Lin Y-S, Hlady V, Andrade JD. Colloids Surf. 1990; 49:289–302.
14. Lin YS, Hlady V. Colloids Surf. B. 1994; 2:481–491.
15. Lin YS, Hlady V. Colloids Surf. B. 1995; 4:65–75.
16. Spijker HT, Bos R, van Oeveren W, de Vries J, Busscher HJ. Colloids Surf. B. 1999; 15:89–97.
17. Lee JH, Khang G, Lee JW, Lee HB. J. Biomed Mater. Res. 1998; 40:180–186. [PubMed: 9549612]
18. Hlady V, Ho CH. Mat-wiss. u. Werkstofftech. 2001; 32:185–192.
19. Welin,-Klintström S, Lestelius M, Liedberg B, Tegvall P. Colloids Surf., B. 1999; 15:81–87.
20. Lin YS, Hlady V, Gölander CG. Colloids Surf. B. 1994; 3:49–62.
21. Walker RA, Cunliffe VT, Whittle JD, Steele DA, Short RD. Langmuir. 2009; 25:4243–4246. [PubMed: 19301839]
22. Loos K, Kennedy SB, Eidelman N, Tai Y, Zharnikov M, Amis EJ, Ulman A, Gross RA. Langmuir. 2005; 21:5237–5241. [PubMed: 15924442]
23. Bos R, de Jonge JH, van de Belt-Gritter B, de Vries J, Busscher HJ. Langmuir. 2000; 16:2845–2850.
24. Ruardy TG, Schakenraad JM, van der Mei HC, Busscher HJ. Surf. Sci. Rep. 1997; 29:1–30.
25. Simon CG Jr, Eidelman N, Kennedy SB, Sehgal A, Khatri CA, Washburn NR. Biomaterials. 2005; 26:6906–6915. [PubMed: 15939467]
26. Lee JH, Jeong BJ, Lee HB. J. Biomed. Mater. Res. 1997; 34:105–114. [PubMed: 8978659]
27. van der Veen M, Norde W, Cohen Stuart M. Colloids Surf. B. 2004; 35:33–40.

28. Corum LE, Hlady V. Biomaterials. 2010; 31:3148–3155. [PubMed: 20149436]
29. Werner C, Maitz MF, Sperling C. J. Mater. Chem. 2007; 17:1–10.
30. Sompayrac, L. How the immune system works. 2nd ed.. Oxford, UK: Blackwell Science; 2003. p. 34-35.
31. Savage B, Rugeri ZM. J. Biol. Chem. 1991; 266:11227–11233. [PubMed: 2040630]
32. Molecular Probes. Alexa Fluor® Succinimidyl Esters. 2007 February 6.
33. Pollard HB, Menard R, Brandt HA, Pazoles CJ, Creutz CE, Ramu A. Anal. Biochem. 1978; 86:761–763. [PubMed: 77646]
34. Hlady V, Buijs J, Jennissen HP. Methods Enzymol. 1999; 309:402–429. [PubMed: 10507038]
35. Caro LC, van Tubergen RP. J. Cell Biol. 1962; 15:173–188. [PubMed: 14018772]
36. Lin YS, Hlady V, Janatova J. Biomaterials. 1992; 13:497–504. [PubMed: 1321678]
37. Liu J, Hlady V. Colloids Surf. B: Biointerf. 1996; 8:25–37.
38. Bhatia SK, Hickman JJ, Ligler FS. J. Am. Chem. Soc. 1992; 114:4432–4433.
39. Tajc SG, Tolbert BS, Basavappa R, Miller BL. J. Am. Chem. Soc. 2004; 126:10508–10509. [PubMed: 15327286]
40. Gao L, McCarthy TJ. Langmuir. 2009; 25:14105–14115. [PubMed: 19627073]
41. Roth CM, Lenhoff AM. Langmuir. 1993; 9:962–972.
42. Gilson MK, Zhou H-X. Annu. Rev. Biophys. Biomol. Struct. 2007; 36:21–42. [PubMed: 17201676]
43. Léveque A. Annales des Mines. 1928; XIII:201–299.
44. Hlady, V.; Ho, CH.; Britt, DW. Interfacial Dynamics. In: Kallay, N., editor. Surfactant Science Series. Vol. Vol. 88. New York: M. Dekker Inc.; 2000. p. 405-418.
45. Dejardin, P.; Vasina, EN. Principles and Practice: Proteins at Solid-Liquid Interfaces. Dejardin, P., editor. Berlin: Springer; 2006. p. 51-73.
46. Evans-Nguyen KM, Tolles LR, Gorkun OV, Lord ST, Schoenfisch HM. Biochemistry. 2005; 44:15561–15568. [PubMed: 16300405]
47. Deshmukh V, Britt DW, Hlady V. Colloids Surfaces B. 2010 submitted.
48. Keogh JR, Wolf MF, Overend ME, Tang L, Eaton JW. Biomaterials. 1996; 17:1987–1994. [PubMed: 8894093]

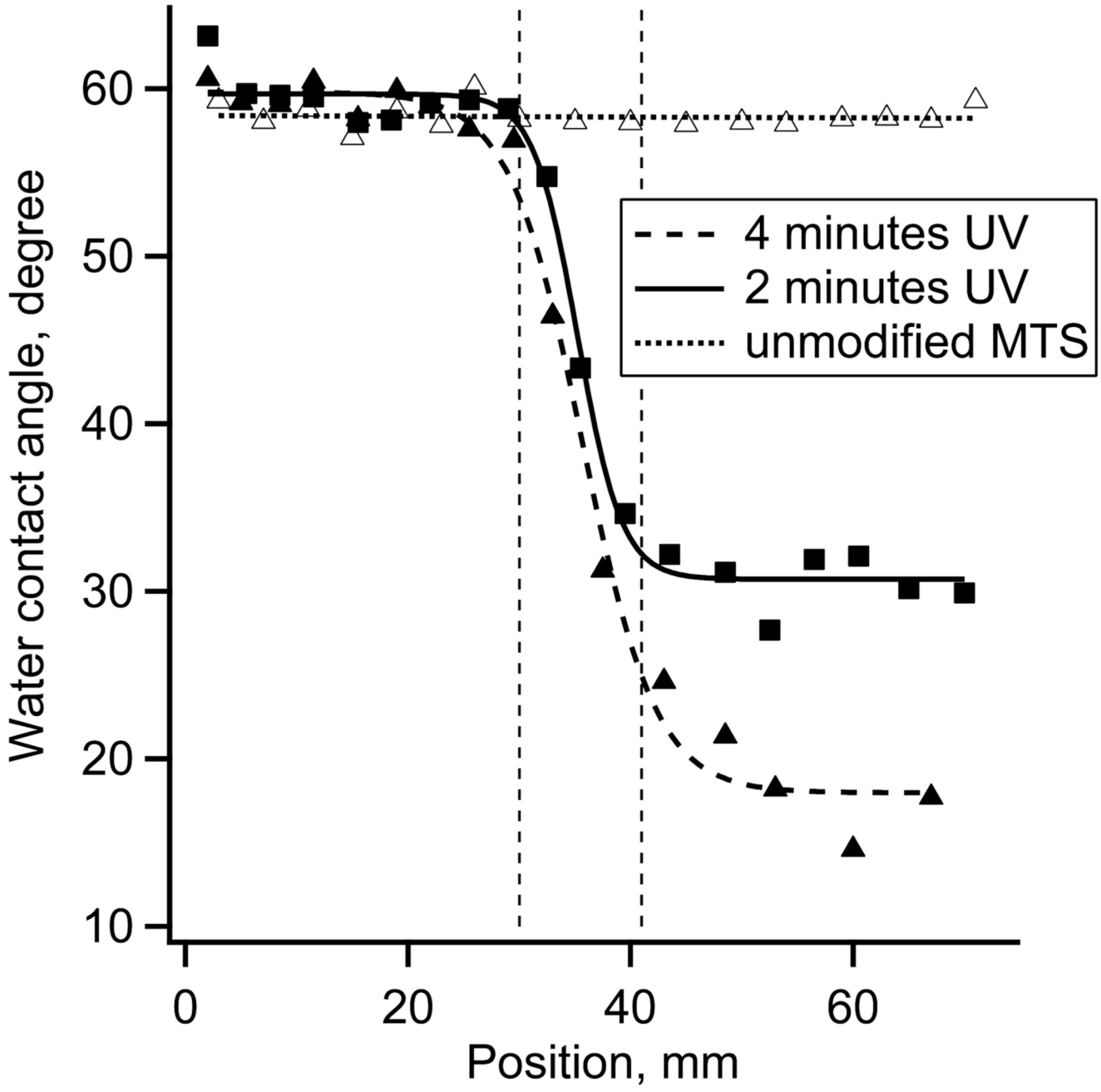

Figure 1.
Receding water contact angles along the surface charge gradient surface for 0, 2 and 4 minutes of UV irradiation.

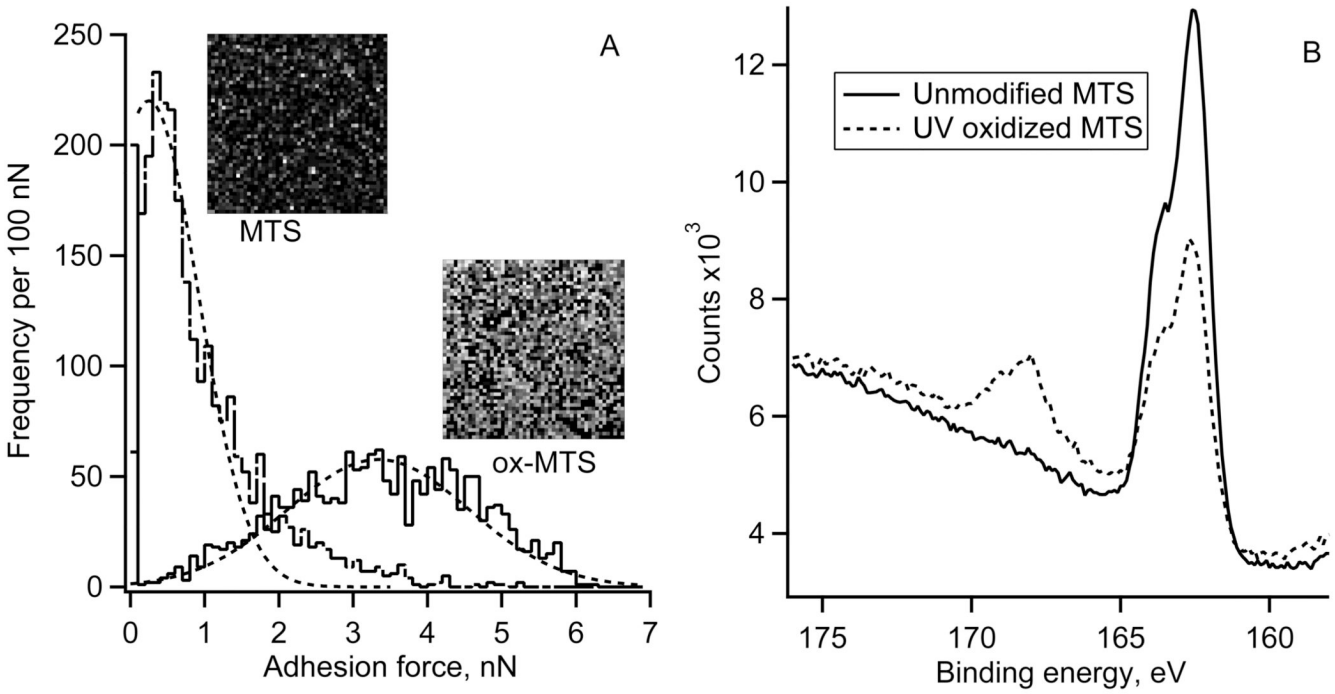

Figure 2.

A) Typical adhesion force histograms and respective adhesion force maps (50 by 50 pixels, each pixel size 200 by 200 nm^2) for an unmodified and UV oxidized (2 minute UV irradiation) MTS monolayer.

B) High-resolution XPS sulfur S2p spectra for unmodified and UV oxidized MTS monolayer (2 minute UV irradiation).

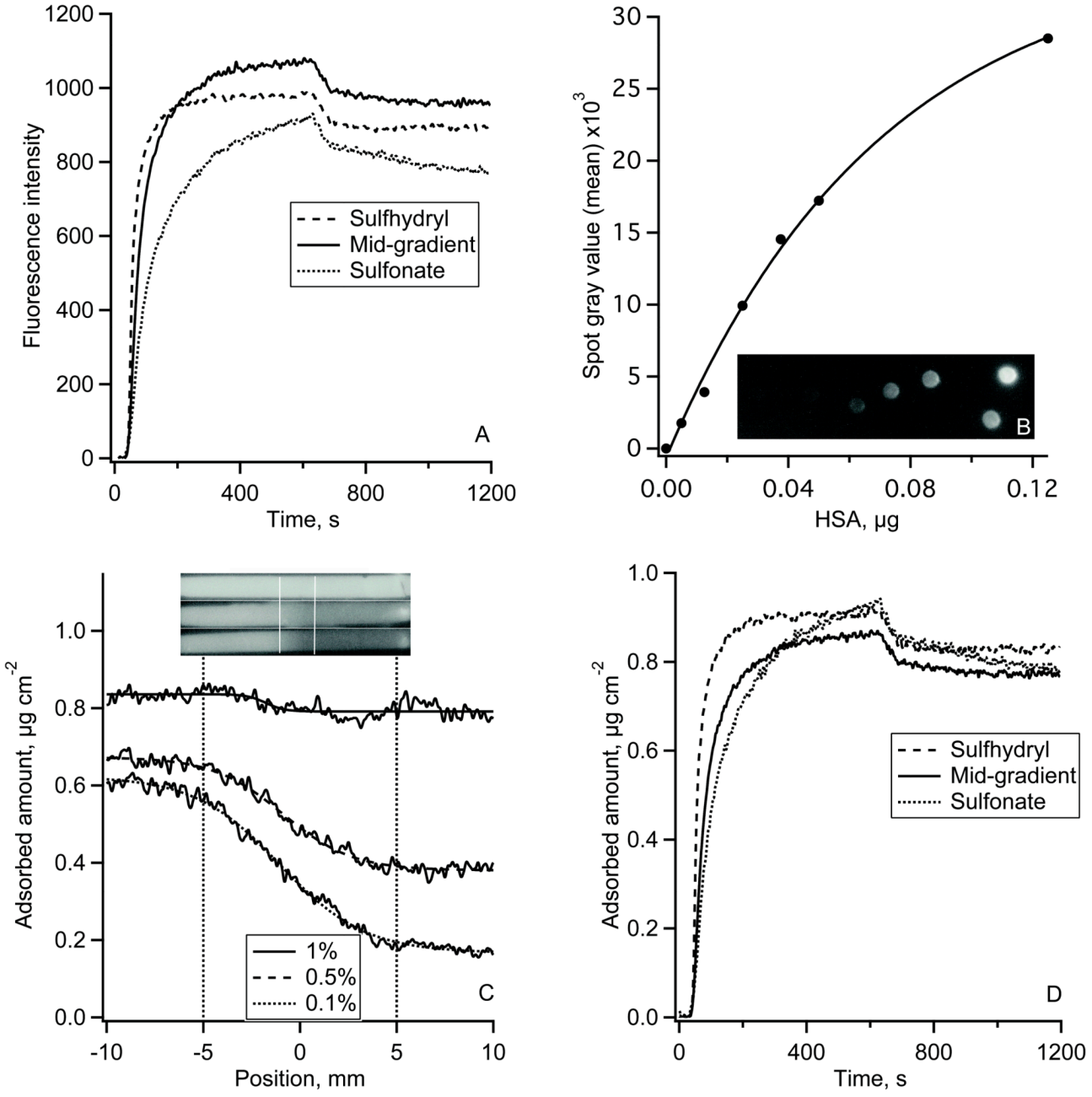

Figure 3.

The adsorption of HSA onto the gradient surface.

(A): Fluorescence intensity traces of Alexa 488-HSA adsorption-desorption kinetics measured on sulfhydryl region, gradient middle and sulfonate-containing region of the gradient in TIRF experiment.

(B): ^{125}I-HSA autoradiography calibration spots and the calibration plot between ^{125}I-HSA mass and the autoradiography image gray values.

(C): Adsorption of ^{125}I-HSA along the gradient surface recorded by autoradiography at 1/100 (top), 1/500 (middle), and 1/1000 (bottom) plasma protein concentration. Top – autoradiography images of ^{125}I-HSA adsorbed onto the whole length of a MTS modified FS

slides with the gradient region in the middle of the slide as indicated. Bottom – calibrated ^{125}I-HSA adsorption profiles along the gradient region.
(D): Alexa 488-HSA adsorption-desorption kinetics from Fig 3A calibrated using autoradiography data.

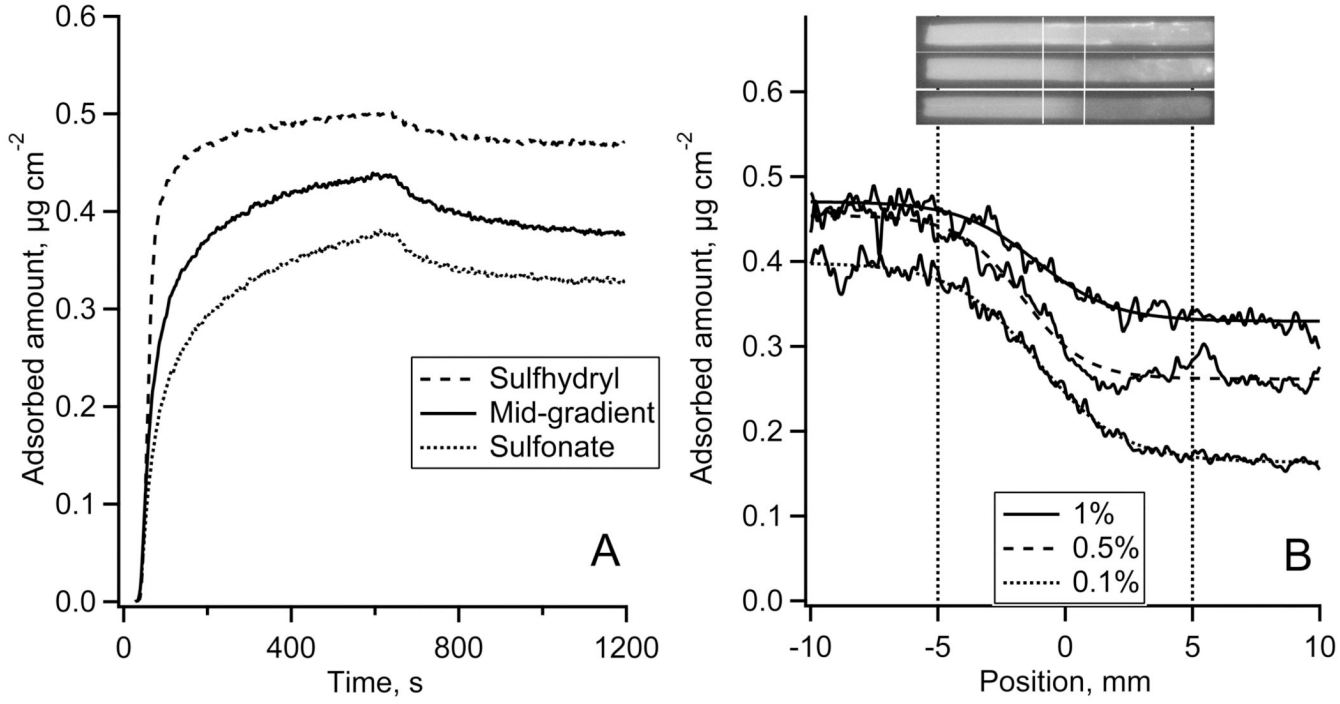

Figure 4.

The adsorption of IgG onto the gradient surface.

(A): Alexa 488-IgG adsorption-desorption kinetics measured in a TIRF experiment and calibrated using autoradiography data from Fig. 4B.

(B): Adsorption of ^{125}I-IgG along the sulfhydryl-to-sulfonate gradient surface recorded by autoradiography at 1/100 (top), 1/500 (middle), and 1/1000 (bottom) plasma protein concentration. Top – autoradiography images of ^{125}I-IgG adsorbed onto the whole length of a MTS modified FS slides with the gradient region in the middle of the slide as indicated. Bottom – calibrated ^{125}I-IgG adsorption profiles along the gradient region.

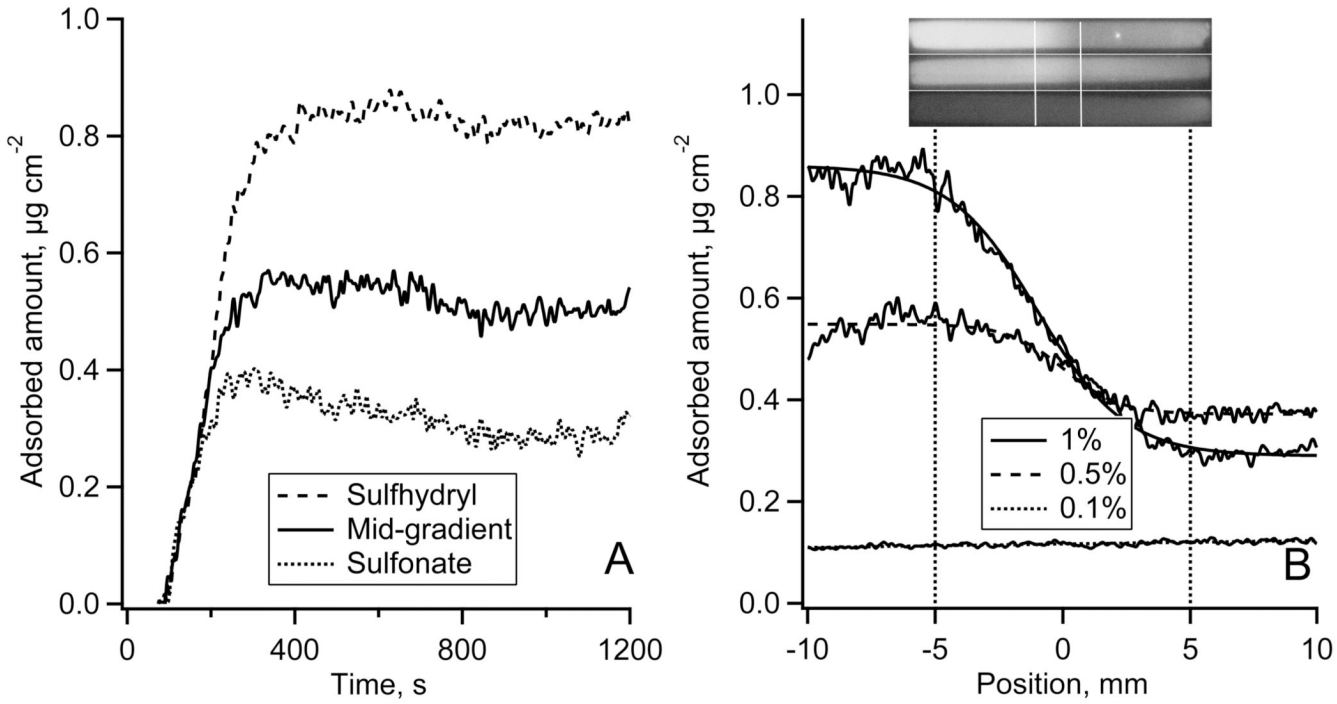

Figure 5.

The adsorption of Fgn onto the gradient surface.

(A): Alexa 488-Fgn adsorption-desorption kinetics measured in TIRF experiment and calibrated using autoradiography data from Fig. 5B.

(B): Adsorption of ^{125}I-Fgn along the sulfhydryl-to-sulfonate gradient surface recorded by autoradiography at 1/100 (top), 1/500 (middle), and 1/1000 (bottom) plasma protein concentration. Top – autoradiography images of ^{125}I-Fgn adsorbed onto the whole length of a MTS modified FS slides with the gradient region in the middle of the slide as indicated. Bottom – calibrated ^{125}I-Fgn adsorption profiles along the gradient region.

TABLE 1

The adsorption parameters of Fgn, HSA, and IgG for the three positions along the surface charge gradient. Each protein concentration was equivalent to the 1/100 of its respective plasma concentration.

		weakly charged, sulhydryl region of gradient	**Center of gradient**	**strongly charged oxidized region of gradient**
Receding water contact angle		60 ± 3°	36 ± 8°	30 ± 4°
HSA	initial rate, $\mu g\ cm^{-2}s^{-1}$	$2.8 \cdot 10^{-2}$	$1.3 \cdot 10^{-2}$	$7.9 \cdot 10^{-3}$
	"Leveque rate" $\mu g\ cm^{-2}s^{-1}$	$3.87 \cdot 10^{-2}$	$4.03 \cdot 10^{-2}$	$4.23 \cdot 10^{-2}$
	k_{off}, s^{-1}	$2.7 \cdot 10^{-2}$	$1.9 \cdot 10^{-2}$	$1.5 \cdot 10^{-2}$
	Γ_{HSA}, $\mu g\ cm^{-2}$	0.83	0.76	0.78
IgG	initial rate, $\mu g\ cm^{-2}s^{-1}$	$8.4 \cdot 10^{-3}$	$7.9 \cdot 10^{-3}$	$7.5 \cdot 10^{-3}$
	"Leveque rate" $\mu g\ cm^{-2}s^{-1}$	$0.88 \cdot 10^{-2}$	$0.91 \cdot 10^{-2}$	$0.96 \cdot 10^{-2}$
	k_{off}, s^{-1}	$0.8 \cdot 10^{-2}$	$0.6 \cdot 10^{-2}$	$0.9 \cdot 10^{-2}$
	Γ_{IgG}, $\mu g\ cm^{-2}$	0.46	0.38	0.32
Fgn	initial rate, $\mu g\ cm^{-2}s^{-1}$	$1.4 \cdot 10^{-3}$	$1.3 \cdot 10^{-3}$	$1.3 \cdot 10^{-3}$
	"Leveque rate" $\mu g\ cm^{-2}s^{-1}$	$1.50 \cdot 10^{-3}$	$1.43 \cdot 10^{-3}$	$1.38 \cdot 10^{-3}$
	k_{off}, s^{-1}	~0	~0	~0
	Γ_{Fgn}, $\mu g\ cm^{-2}$	0.83	0.51	0.30